ARL-TR-9014 ● SEP 2020

DEVCOM ARMY RESEARCH LABORATORY

Study of Advanced Thermal Barrier Coatings and Calcia–Magnesia–Alumino–Silicate (CMAS) Interactions

by Alex Berendt, Anindya Ghoshal, Rick Reidy, Michael Walock, and Muthuvel Murugan

NOTICES

Disclaimers

The findings in this report are not to be construed as an official Department of the Army position unless so designated by other authorized documents.

Citation of manufacturer's or trade names does not constitute an official endorsement or approval of the use thereof.

Destroy this report when it is no longer needed. Do not return it to the originator.

ARL-TR-9014 ● SEP 2020

Study of Advanced Thermal Barrier Coatings and Calcia–Magnesia–Alumino–Silicate (CMAS) Interactions

Alex Berendt and Rick Reidy
University of North Texas

Anindya Ghoshal, Michael Walock, and Muthuvel Murugan
Vehicle Technology Directorate, CCDC Army Research Laboratory

REPORT DOCUMENTATION PAGE

Form Approved
OMB No. 0704-0188

1. REPORT DATE *(DD-MM-YYYY)*	2. REPORT TYPE	3. DATES COVERED
September 2020	Technical Report	22 May 2019–10 August 2019

4. TITLE AND SUBTITLE
Study of Advanced Thermal Barrier Coatings and Calcia–Magnesia–Alumino–Silicate (CMAS) Interactions

5a. CONTRACT NUMBER

5b. GRANT NUMBER

5c. PROGRAM ELEMENT NUMBER

6. AUTHOR(S)
Alex Berendt, Anindya Ghoshal, Rick Reidy, Michael Walock, and Muthuvel Murugan

5d. PROJECT NUMBER

5e. TASK NUMBER

5f. WORK UNIT NUMBER

7. PERFORMING ORGANIZATION NAME(S) AND ADDRESS(ES)
CCDC Army Research Laboratory
ATTN: FCDD-RLV-P
Aberdeen Proving Ground, MD 21005

8. PERFORMING ORGANIZATION REPORT NUMBER
ARL-TR-9014

9. SPONSORING/MONITORING AGENCY NAME(S) AND ADDRESS(ES)

10. SPONSOR/MONITOR'S ACRONYM(S)

11. SPONSOR/MONITOR'S REPORT NUMBER(S)

12. DISTRIBUTION/AVAILABILITY STATEMENT
Approved for public release; distribution is unlimited.

13. SUPPLEMENTARY NOTES

14. ABSTRACT
The infiltration and adhesion of molten particulates is a significant problem for gas-turbine engines (GTEs) operating in particle-laden environments. The resultant glassy calcia–magnesia–alumino–silicate coating on hot-section components can lead to early GTE failure and decreased rotorcraft flight time. Between 2000 and 2013, the US military lost 26 rotorcraft, costing $533 million, due to operating in brownout conditions. A quantitative understanding of the chemical reaction kinetics between ingested particulates and thermal barrier coatings (TBCs) is key to developing effective mitigation strategies that limit Army exposure to this environmental risk. To this end, we have mixed TBC powders with a synthetic sand, AFRL-02, to study the reaction kinetics. After analysis with a scanning electron microscope (SEM), equipped with an energy-dispersive X-ray spectrometer (EDS) for elemental analysis, the powders were melted at 1,300 °C for 4 h. The resultant "glass" was subsequently imaged/analyzed with SEM-EDS. In addition, X-ray diffraction and differential scanning calorimetry (up to 1,400 °C) data are also being collected on the powder mixtures to aid in identifying new phases and reactive species being formed. The information will be used to develop new TBCs with sandphobic qualities for increased reliability/durability of Army vertical-takeoff-and-landing engines.

15. SUBJECT TERMS
sandphobic, thermal barrier coatings, adhesion, calcia–magnesia–alumino–silicate, CMAS, blended ceramic composite

16. SECURITY CLASSIFICATION OF:			17. LIMITATION OF ABSTRACT	18. NUMBER OF PAGES	19a. NAME OF RESPONSIBLE PERSON
a. REPORT	b. ABSTRACT	c. THIS PAGE			Anindya Ghoshal
Unclassified	Unclassified	Unclassified	UU	23	19b. TELEPHONE NUMBER (Include area code) 410-278-7358

Contents

List of Figures

List of Tables

1. Introduction

Gas-turbine engine (GTE) operation in particle-laden environments leads to infiltration and adhesion of molten calcia–magnesia–alumino–silicate (CMAS) in thermal barrier coatings (TBCs) on hot-section components. Fine particles pass through cold sections and enter the combustor, where they melt and impinge on high-pressure turbine components. Molten particles then adhere to the TBC, followed by infiltration of the porous coatings, leading to further degradation of the TBC.

The industry standard, 8-mol% yttria-stabilized zirconia (8YSZ) TBC, is highly vulnerable to CMAS attack and eventually fails, causing early GTE failure and reduced flight time of vertical-takeoff-and-landing aircraft. The production of a more sandphobic TBC would allow increased efficiency, engine performance, and flight time. To create a sandphobic TBC, we must first understand which phases are changing and which chemical reactions are taking place.

We designed experiments to analyze the chemical reaction kinetics between molten CMAS and the TBCs to better understand the melt interactions with several compositions of TBCs. We also analyzed the effects of varying TBC composition on adhesion by comparing interfacial strength and area covered by CMAS.

TBC failure is caused by molten CMAS infiltration. In previous works it was shown that anhydrite ($CaSO_4$) forms and introduces residual stresses.[1–3] These stresses are caused by coefficient of thermal expansion (CTE) differences that can lead to crack formation and growth that worsens with increasing cycles.[4]

Protective layers such as calcium zirconate and a kimzeyite garnet also form.[3] Local melt chemistry affects the formation of these protective layers and other reactions. When the yttria is leached out, local melt chemistry changes, as do the phases present.[4] Calcium replaces yttria, and the zirconia is no longer tetragonal prime (t') but becomes cubic. This phase transformation makes the zirconia less stable at lower temperatures and causes an increase in thermal conductivity. The formation of new reactive species and protective layers is also beneficial. When these layers form at the surface, they act as a barrier between the TBC and CMAS on the surface.

2. Methods

2.1 Adhesion Experiment

TBCs of various compositions were deposited on Inconel pucks using air plasma spraying. Once the TBCs were deposited, sand slurry was brushed on the surface and two pucks of the same composition were pushed together for 30 s. When the slurry was dry, the samples were placed in a box furnace for various amounts of time and temperature.

The samples were then tested with an Elcometer 510 Model adhesion strength tester to measure the strength of the interface at which failure occurs.

2.2 Bulk Reaction Experiment

TBC powders were weighed and mixed with an equal weight of AFRL-02 test dust at (50/50 wt%) mixture. Then 1.5 g of the powder/test-dust mix were placed in a crucible and ramped in a box furnace at 5 °C/min up to 1,300 °C, where the sample was held for 4 h then ramped back to room temperature at 5 °C/min.

After the 1.25-inch sample was removed from the furnace, it was set in epoxy. The sample was then polished with a Struers TegraPol-21 polisher, TegraForce-5 polisher head, and a TegraDoser-5 dosing system (first with 300-grit sandpaper, then 420-, 600-, and 1,200-grit ExTec silicon carbide [SiC] paper). Then the sample was polished with a Struers MD Largo pad with a 15-µm diamond abrasive followed by an Allied Pan B pad with 9-µm diamond abrasive for 10 min each, Buehler Trident with 3-µm diamond abrasive for 8 min, Struers MD Dac with 1-µm diamond abrasive for 1.5 min, and finally a Struers MD Chem pad with 0.02-µm colloidal silica abrasive for 3 min. The SiC paper was run at 300 rpm (head/base), and the polishing pads were run at 150 rpm (head/base), all with a force of 25 N per sample, or 150 N for the entire holder of six samples.

These samples were also characterized using a Hitachi 3500 scanning electron microscope (SEM) and energy-dispersive X-ray spectroscopy (EDS). SEM and EDS were used to characterize the TBC powders, TBC powder/test-dust mixture, and the polished mixture melt. The loose powders were placed on carbon tape and the polished samples in a holder for SEM and EDS.

2.3 Results

2.3.1 Adhesion Experiment

Some of the adhesion results are tabulated in Table 1.

Table 1 Adhesion experiment parameters

Sample	Composition	Temp. (°C)	Time (min)	Adhesion Strength (MPa)	Dry weight (g)	Wet weight (g)	Sintered weight (g)
A1100-30D	8YSZ	1100	30	n/a	35.766	36.070 (.008%)	35.873 (.003%)
S5	8YSZ+32vol % Gd_2O_3	900	1200	0.13	34.492	35.039 (.016%)	35.825 (.039%)
S10	8YSZ+8vol% Gd_2O_3	700	1200	0.13	35.392	35.530 (.004%)	35.649 (.007%)

Sample A1100-30D (Fig. 1) is composed of 8YSZ and was heat treated at 1,100 °C for 30 min. Once this sample was pulled apart with the adhesion tester, both TBC surfaces seemed to be covered in CMAS. This leads us to believe that failure occurred at the sand–sand interface.

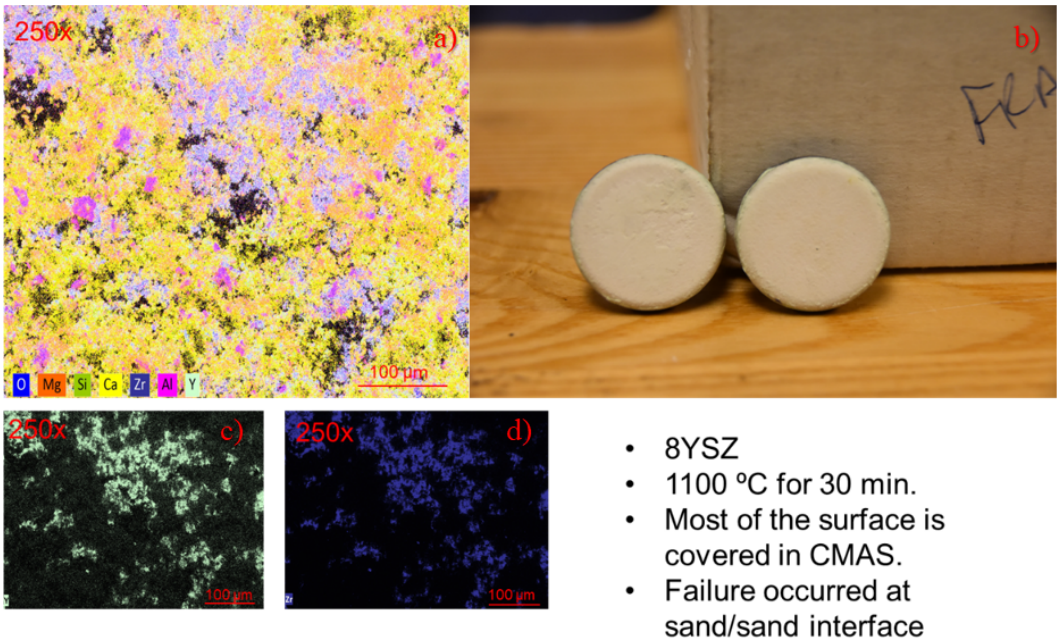

Fig. 1 Sample A1100-30D: a) EDS map, b) digital single-lens reflex (DSLR) camera image, c) yttrium EDS map from image (a), and d) zirconium EDS map from image (a)

Sample S5 (Fig. 2) was composed of 8YSZ-32-vol% gadolinium(III) oxide (Gd_2O_3) and heat treated at 900 °C for 1,200 min (20 h). The DSLR image of sample S5 looks drastically different from the DSLR image of Sample A1100-30D. Much more TBC is visible in this sample because failure occurred at the sand–TBC interface rather than at the sand–sand interface.

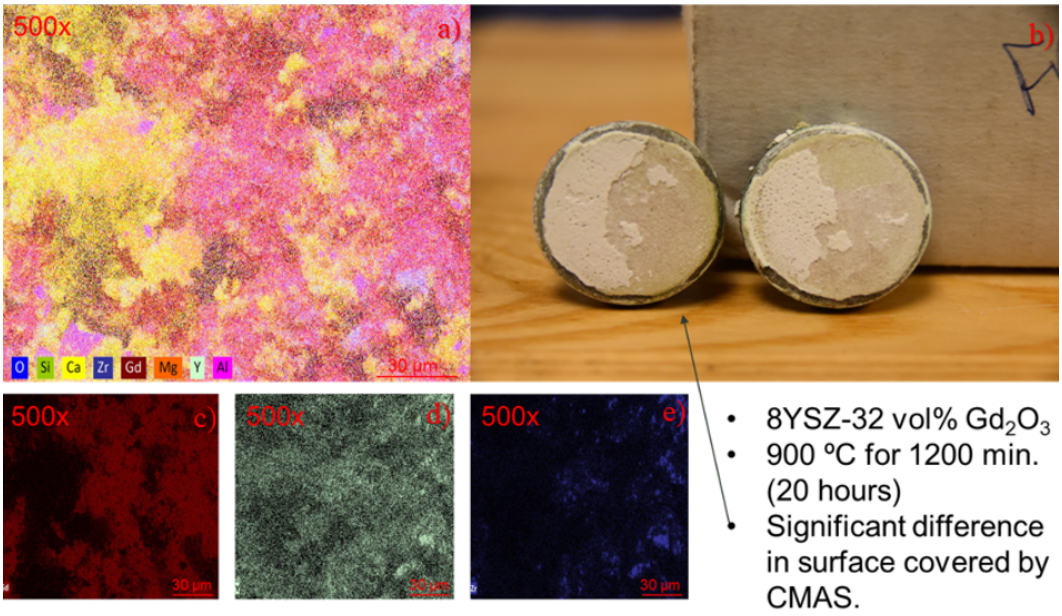

Fig. 2 Sample S5: a) EDS map, b) DSLR image, c) gadolinium EDS map from image (a), d) yttrium EDS map from image (a), and e) zirconium EDS map from image (a)

Sample S10 (Fig. 3) was composed of 8YSZ-8-vol% Gd_2O_3 and heat treated at 700 °C for 1,200 min (20 h). S10 is very similar to S5, but there seems to be slightly less TBC visible in S10.

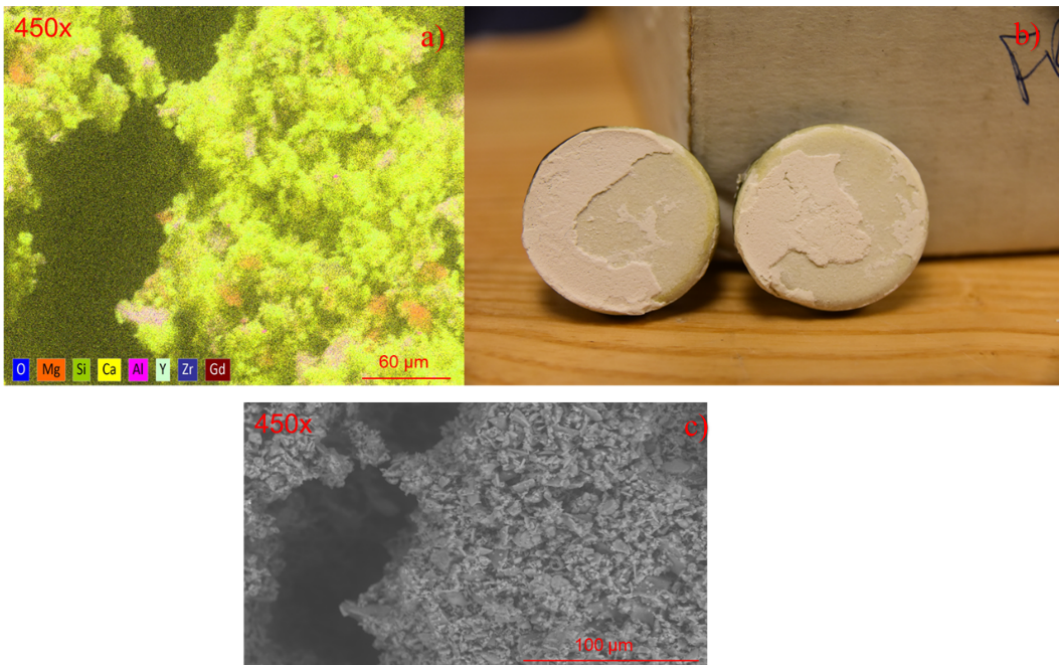

Fig. 3 Sample S10: a) EDS map, b) DSLR image, and c) SEM image

The adhesion of the sand was very weak, as expected. Failure occurred at the sand–TBC interface or sand–sand interface in all samples. Sample A1100-30D was broken in shipping; therefore, no adhesion strength was available, but the adhesion of the other samples was very low as well. An adhesion strength of 0.13 MPa is approximately 2 orders of magnitude weaker than the adhesion strength of a TBC on to the substrate, which is 15–25 MPa.[5] The sand coverage is noticeably different in S5 and S10 compared with A1100-30D, which has much less TBC visible in the DSLR image than samples S5 and S10. These samples were all tested with slightly different conditions, but none of the samples reached the melting temperature of CMAS (T_m = 1,220 °C). The other key difference in these samples was the composition of the TBCs. The CMAS seemed to adhere less to the TBCs with higher volume-percent gadolinia.

2.3.2 Bulk Reaction Experiment

The premelt mixture of this sample in Fig. 4a shows the 8YSZ particles in the CMAS. After the heat treatment the YSZ particles seem to break apart, as seen in Fig. 4d and 4e. This was possibly the YSZ dissolving in the molten CMAS since the sample was held at 1,300° for 4 h.

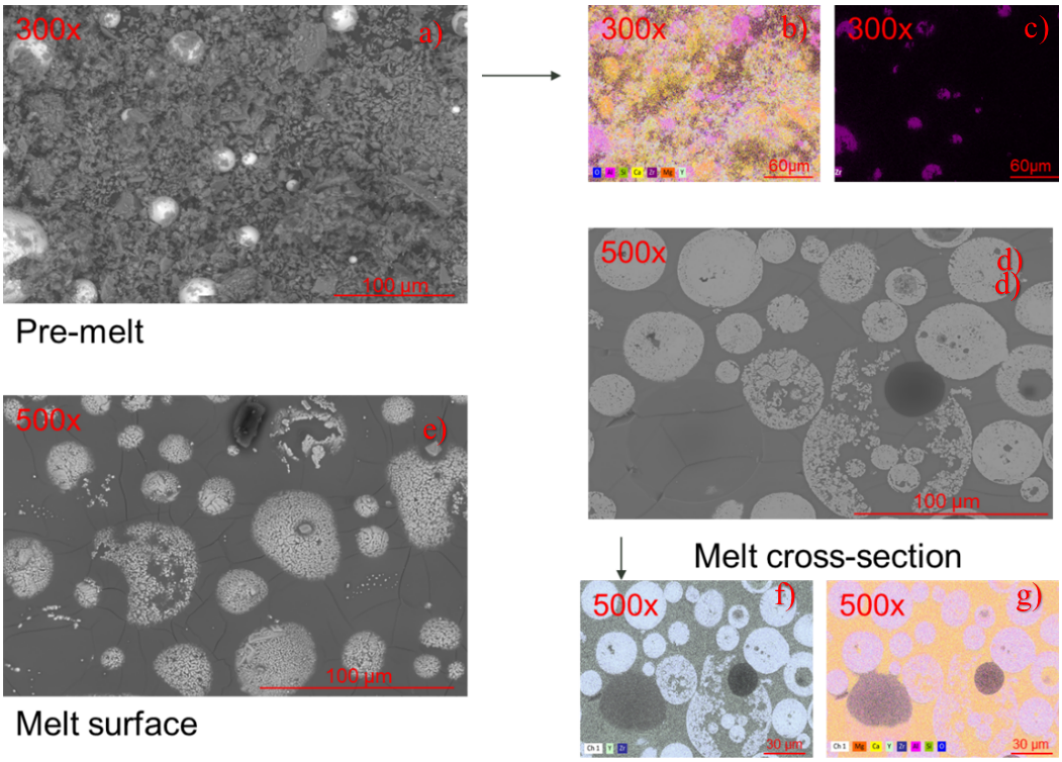

Fig. 4 8YSZ-AFRL-02: a) SEM image of premelt mixture, b) EDS map of image (a), c) zirconium EDS map of image (a), d) SEM image of cross section after melt, e) SEM image of melt surface, f) yttrium and zirconium EDS map of image (d), and g) EDS map of image (d)

Figures 5–10 all show similar behavior of the YSZ particles breaking apart. Some YSZ particles are already hollow while others are dense. Some of the YSZ particles have slight porosity that may be hollowing of the particle since they look different from the previously hollow particles. The most important difference in these samples as compared with the 8YSZ-AFRL-02 is the increasing gadolinia content. The gadolinia is in localized pockets before heat treatment, but after treatment the gadolinia is more homogeneous in the samples. The gadolinia was detected in the same area as the CMAS, which could be evidence of the gadolinia dissolving in the molten CMAS. Small black pockets are also seen in most of the cross-section SEM images, which is most likely contamination from polishing. The small diamond abrasives were encompassed by the epoxy used to hold the samples in place.

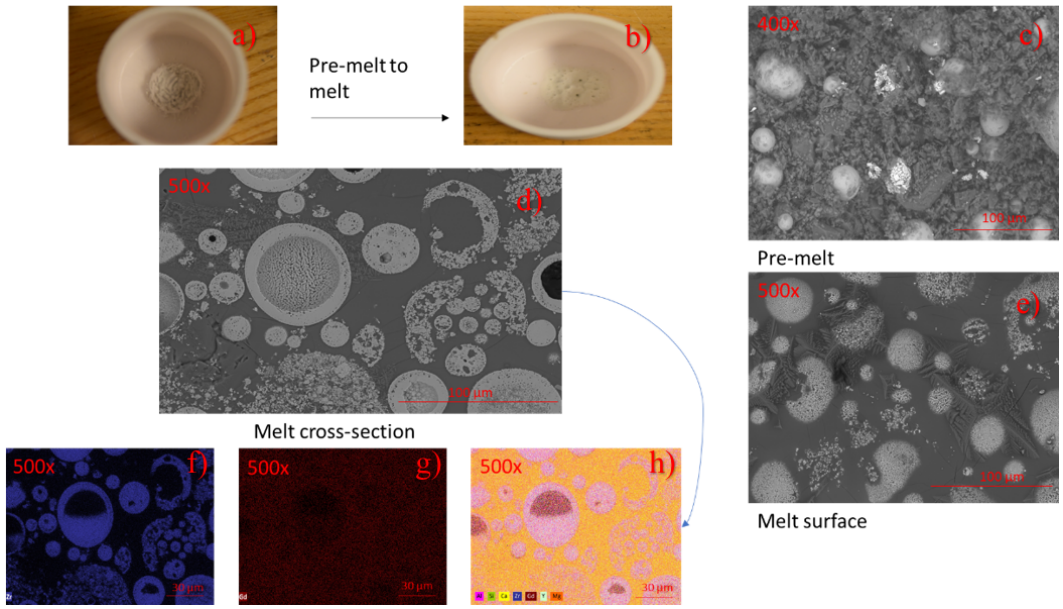

Fig. 5 8YSZ-2-vol% Gd_2O_3-AFRL-02: a) premelt powder in crucible, b) powder after melt in crucible, c) SEM image of pre-melt mixture, d) SEM image of cross section after melt, e) SEM image of melt surface, f) zirconium EDS map of image (d), g) gadolinium EDS map of image (d), and h) EDS map of image (d)

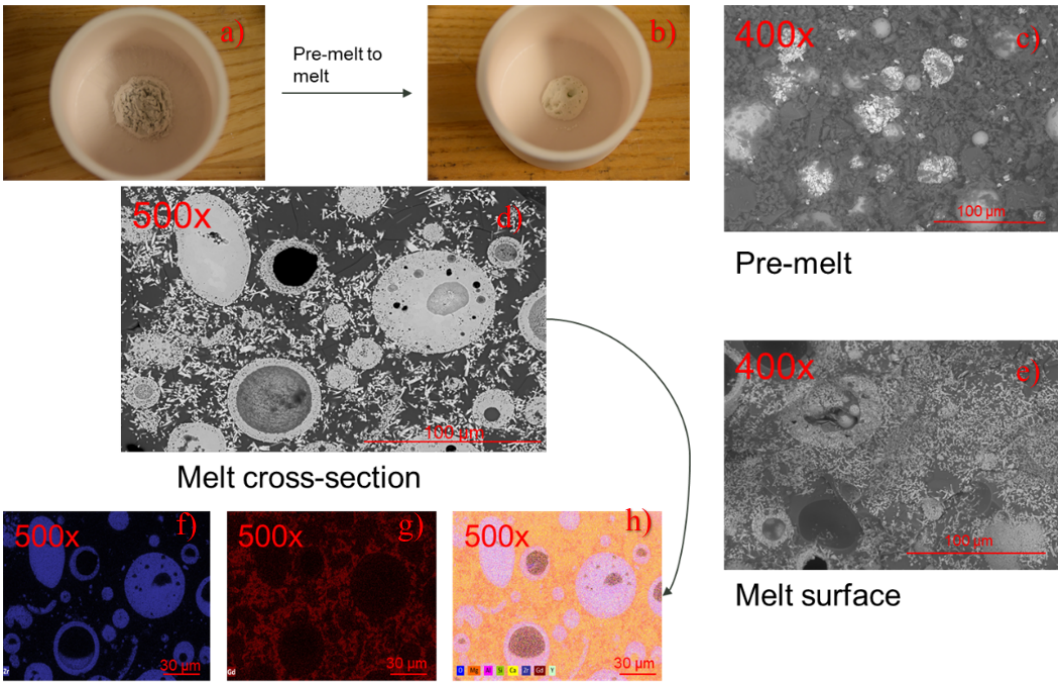

Fig. 6 8YSZ-8-vol% Gd_2O_3-AFRL-02: a) premelt powder in crucible, b) powder after melt in crucible, c) SEM image of pre-melt mixture, d) SEM image of cross section after melt, e) SEM image of melt surface, f) zirconium EDS map of image (d), g) gadolinium EDS map of image (d), and h) EDS map of image (d)

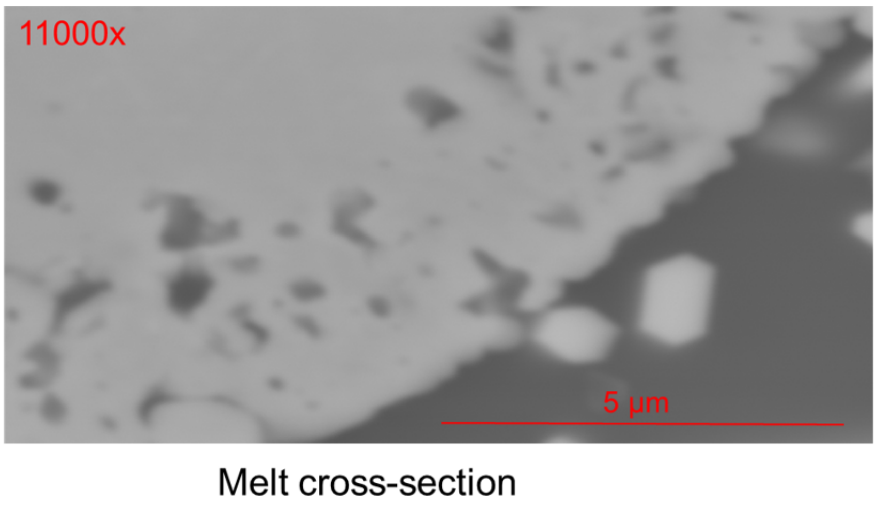

Fig. 7 8YSZ-8-vol% Gd_2O_3-AFRL-02: a) SEM image of sample cross section after melt, b) EDS map of image (a), and c) zirconium, gadolinium, and yttrium EDS map of image (a)

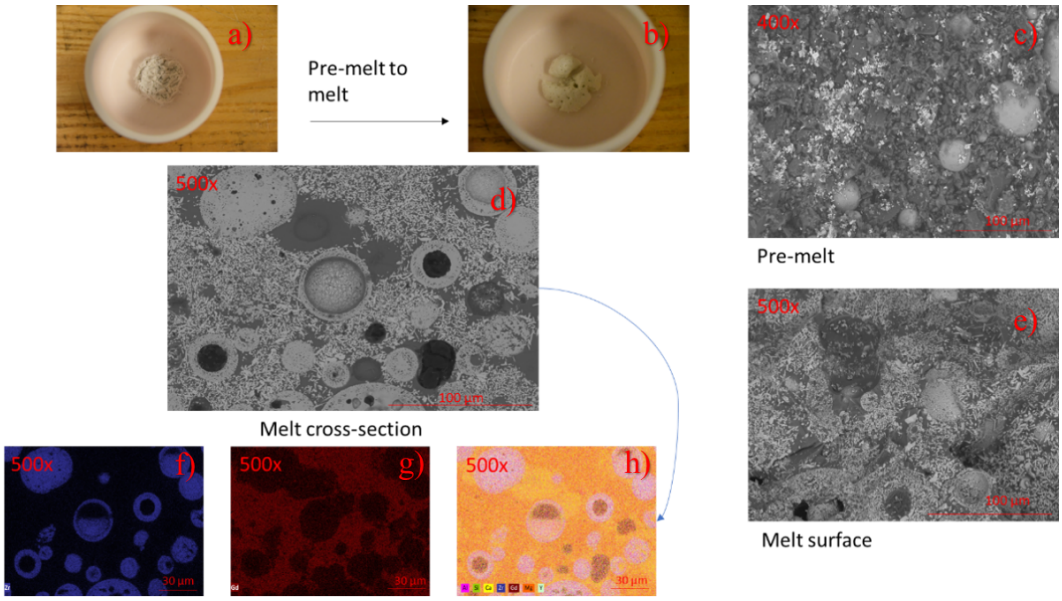

Fig. 8 8YSZ-17-vol% Gd_2O_3-AFRL-02: a) premelt powder in crucible, b) powder after melt in crucible, c) SEM image of pre-melt mixture, d) SEM image of cross section after melt, e) SEM image of melt surface, f) zirconium EDS map of image (d), g) gadolinium EDS map of image (d), and h) EDS map of image (d)

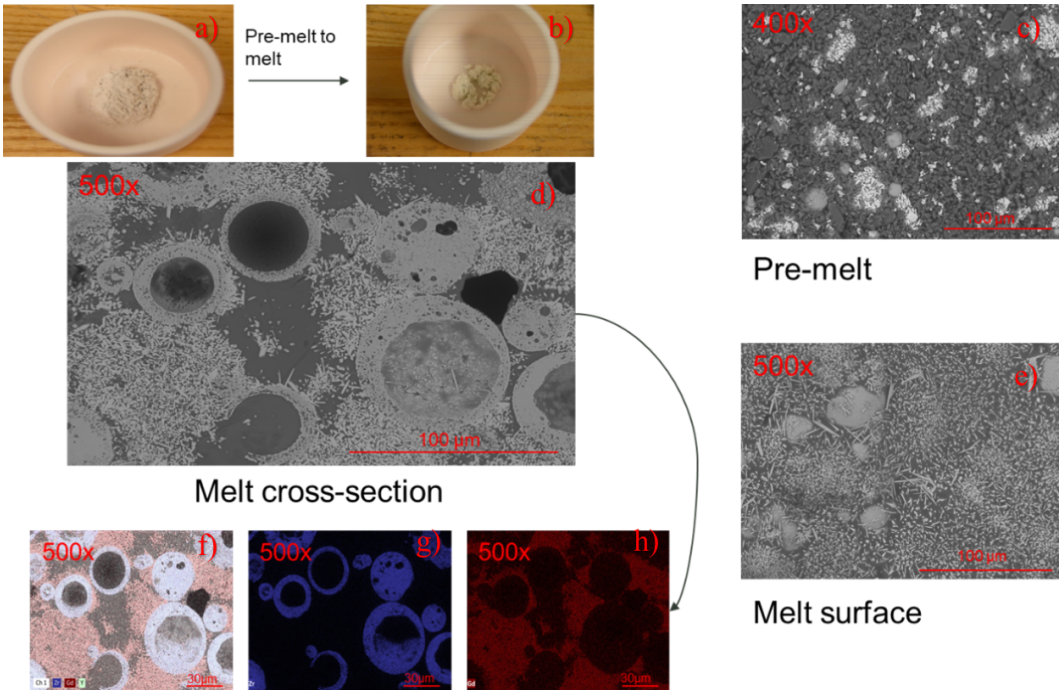

Fig. 9 8YSZ-32-vol% Gd_2O_3-AFRL-02: a) premelt powder in crucible, b) powder after melt in crucible, c) SEM image of pre-melt mixture, d) SEM image of cross section after melt, e) SEM image of melt surface, f) yttrium, zirconium, and gadolinium EDS map of image (d), g) zirconium EDS map of image (d), and h) gadolinium EDS map of image (d)

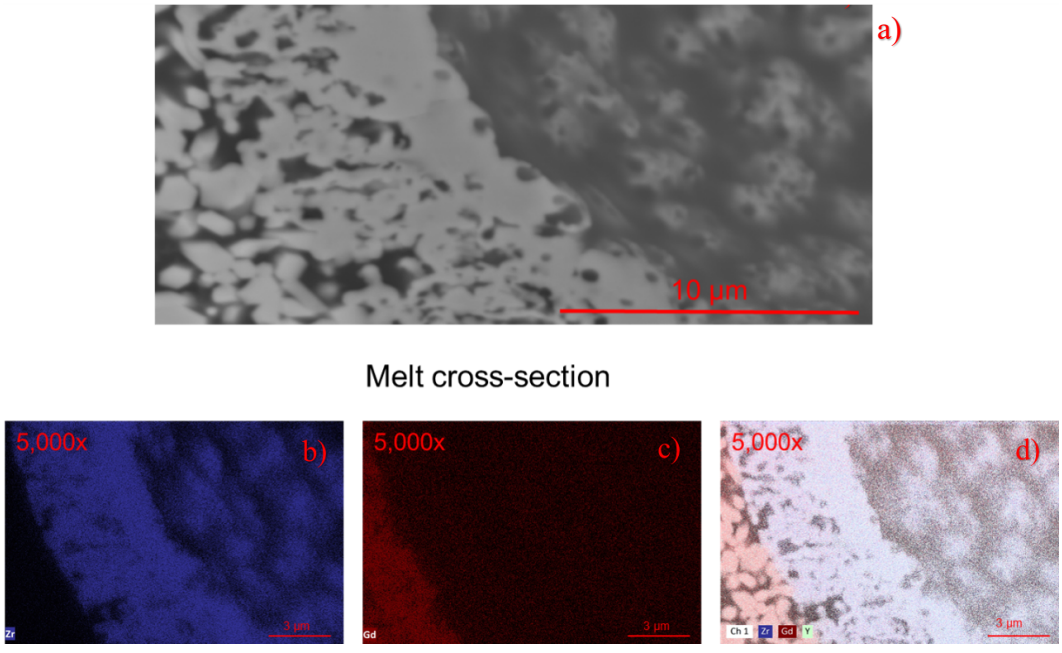

Fig. 10 8YSZ-32-vol% Gd_2O_3-AFRL-02: a) SEM image of sample cross section after melt, b) zirconium EDS map of image (a), c) gadolinium EDS map of image (a), and d) zirconium, gadolinium, and yttrium EDS map of image (a)

Figures 7 and 10 show SEM images of gadolinia at a much higher magnification. These SEM images were taken at the boundary of a YSZ particle to analyze a possible diffusion layer. In Figs. 7c and 10c, diffusion is seen between the gadolinium and zirconium. These EDS spectra could be evidence of a protective layer forming. While looking for the possible formation of a protective layer, small hexagons were viewed near the YSZ particle. These small hexagons appeared as gadolinium in EDS and ranged from 0.5 to 2 μm. These small gadolinia particles underwent a large change in particle size, as the original size was approximately 33 μm. The cause of this could be the gadolinia dissolving in the molten CMAS and reprecipitating out with a much smaller particle size. These phenomena could lead to changes in adhesion as well as prevention of undesirable phase changes.

Figure 11 is gadolinia mixed with AFRL-02 and it shows behavior similar to the gadolinia mixed with YSZ and AFRL-02 in previous samples. The gadolinia is localized in the premelt in Fig. 11c, but after heat treatment the gadolinia is more homogeneous. Figure 12 shows the samaria (Sm_2O_3) and AFRL-02 sand mix, and shows similar behavior to gadolinia, except the samaria begins with a smaller particle size. Change in particle size is not as noticeable in samaria, but image Fig. 12f shows the samaria becoming more homogenous in the CMAS.

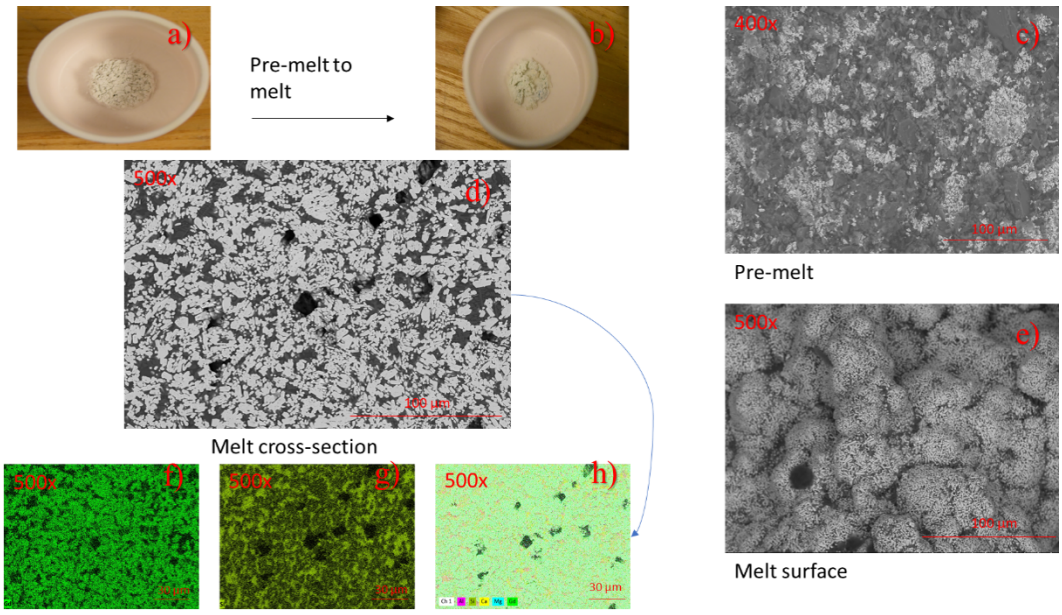

Fig. 11 Gd_2O_3-AFRL-02: a) premelt powder in crucible, b) powder after melt in crucible, c) SEM image of premelt mixture, d) SEM image of cross section after melt, e) SEM image of melt surface, f) gadolinium EDS map of image (d), g) silicon EDS map of image (d), and h) EDS map of image (d)

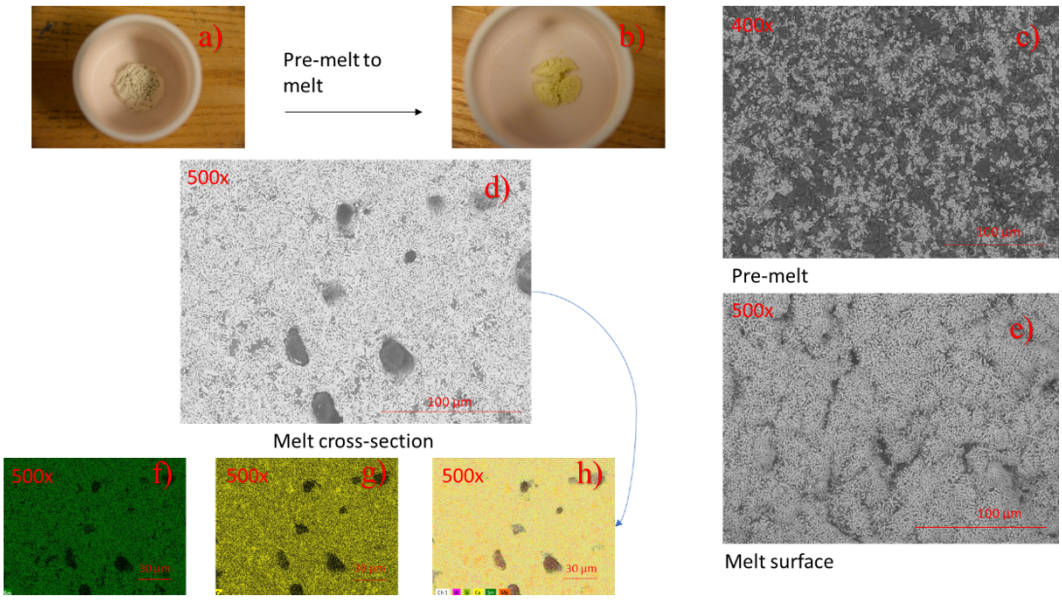

Fig. 12 Sm_2O_3-AFRL-02: a) premelt powder in crucible, b) powder after melt in crucible, c) SEM image of premelt mixture, d) SEM image of cross section after melt, e) SEM image of melt surface, f) samarium EDS map of image (d), g) calcium EDS map of image (d), and h) EDS map of image (d)

The melts in Fig. 13 all show different behavior based off composition. Samples in Figs 13b, c, e, and g all cracked after cooling, and Fig. 13c shows the samaria turning yellow. These samples seem to show more porosity and cracking with increasing gadolinia content. Once the samples hit 17-vol% gadolinia in Fig. 13b, the samples began to crack, which may be due to lower adhesion strength because of the amount of gadolinia. Figs. 13 a, d, and f are all uncracked but seem to wet the surface of the crucible in different ways. The 2-vol% gadolinia in Fig. 13d seems to wet the surface more than 8YSZ in Fig. 13a, but the sample with 8-vol% gadolinia in Fig. 13f seems to wet the surface less.

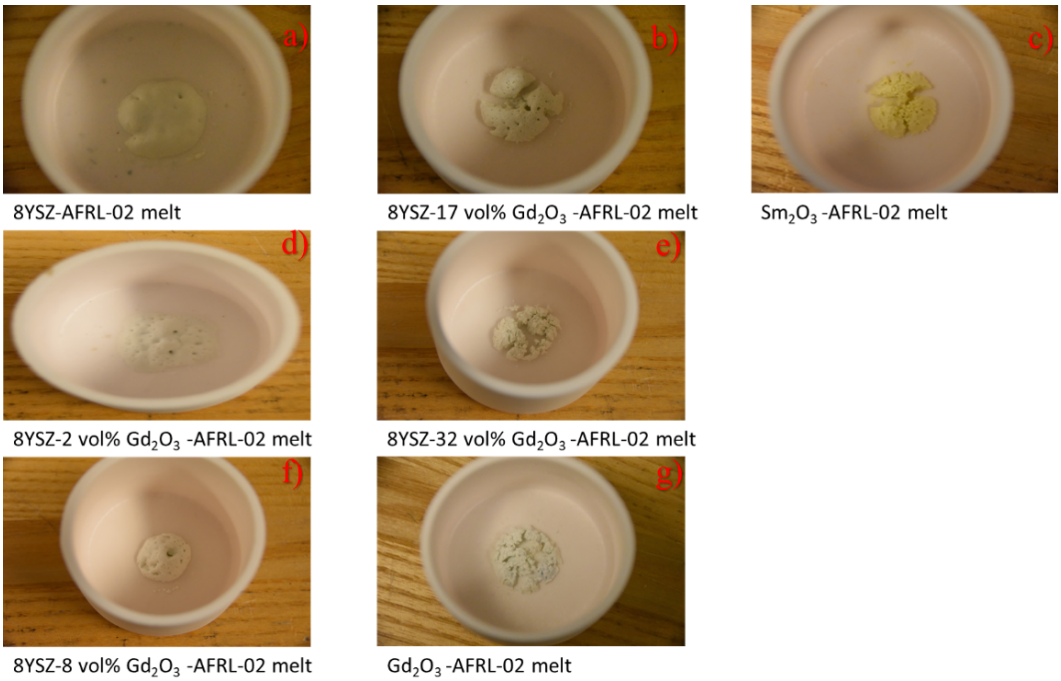

Fig. 13 Melt comparison

3. Conclusions

The adhesion strength of the sand–TBC interface is weaker when gadolinia is present. Since the sand–sand interface broke in the 8YSZ TBC sample, the sand adheres more to the surface of the samples than to the sand itself. In Fig. 1, the DSLR images show that the sand–sand interface broke because almost no TBC is visible. The gadolinia TBC samples in Fig. 2 and Fig. 3 show that the sand–TBC interface failed first. This could be very valuable for the development of sandphobic TBCs. It is unknown exactly how much the volume percent of gadolinia in the TBC affects the adhesion of the sand to the TBC surface. The decrease in adhesion of the sand to TBC surface will aid in decreasing buildup of CMAS, which may decrease the infiltration of CMAS in the TBC.

Through the bulk reaction experiments we were able to study the chemical reaction kinetics. In Figs. 7 and 9, high-magnification SEM images show small particles that show up as gadolinium in EDS. As mentioned, this could be evidence of gadolinia dissolving in the CMAS melt and reprecipitating out with a much smaller particle size. This could be beneficial if the gadolinia particle size can be controlled, as the small particles may affect the surface energy of the molten CMAS on the TBC surface. The surface energy increasing could change how the molten CMAS wets the surface, which could decrease adhesion of CMAS to TBC.

The YSZ did not dissolve as much as expected, but YSZ particles were seen breaking apart in the molten CMAS. Some hollowing of the YSZ particle may have occurred, but it is hard to say definitively since some YSZ particles were already hollow.

4. Future Work

Further adhesion test will be run with different parameters. The same samples will be tested but with all at the same temperature and length of cycle. This method will make it easier to compare the samples, especially between samples with gadolinia and without. We will also perform surface analysis to compare samples with gadolinia to measure the effect on TBC coverage compared with the amount of gadolinia in the samples.

The bulk reaction experiment will be changed slightly by increasing the box furnace cycle. Instead of holding the sample at temperature for 4 h, we will hold them at temperature for 24 h. Increasing the furnace cycle will allow more time for diffusion coupled with further postprocessing to allow us to better detect the formation of protective layers. We will also perform X-ray diffraction and differential scanning calorimetry to better detect new phases and reactive species.

5. References

1. Ghoshal A, Walock MJ, Murugan M, Mock C, Bravo L, Pepi M. Governing parameters influencing CMAS adhesion and infiltration into environmental/thermal barrier coatings in gas-turbine engines. Proc ASME Turbo Expo 2019: Turbomachinery Technical Conference and Exposition. 2019 Nov 5 [accessed 2020 May 5]. https://doi.org/10.1115/GT2019-92000.

2. Mock C, Walock MJ, Wright A, Nieto A, Ghoshal A, Murugan M, Pepi M. Rare-earth oxides blended with yttria-stabilized zirconia thermal barrier coatings for improved resistance to sand adherence and calcia-magnesia-alumino-silicate (CMAS) infiltration. ASME; 2019 June 17. ASME Paper No.: GT2019-90395, V006T24A006.

3. Braue W, Mechnich P. Recession of an EB-PVD YSZ coated turbine blade by $CaSO_4$ and Fe, Ti-rich CMAS-type deposits. J Am Ceram Soc. 2011. https://doi.org/10.1111/j.1551-2916.2011.04747.x.

4. Witz G, Shklover V, Steurer W, Bachegowda S, Bossmann HP. High-temperature interaction of yttria-stabilized zirconia coatings with CaO-MgO-Al_2O_3-SiO_2 (CMAS) deposits. Surf Coat Tech. 2015. https://doi.org/10.1016/j.surfcoat.2009.07.034.

5. Ghasemi R, Vakilifard H. Plasma-sprayed nanostructured YSZ thermal barrier coatings: thermal insulation capability and adhesion strength. Ceramics International. 2017;43(12):8556–8563.

List of Symbols, Abbreviations, and Acronyms

8YSZ	8-mol% yttria-stabilized zirconia
AFRL-02	synthetic sand
$CaSO_4$	anhydrite
CMAS	calcia–magnesia–alumino–silicate
CTE	coefficient of thermal expansion
DSLR	digital single-lens reflex
EDS	energy-dispersive X-ray spectroscopy
Gd_2O_3	gadolinium(III) oxide
GTE	gas-turbine engine
SEM	scanning electron microscope
SiC	silicon carbide
Sm_2O_3	samaria
TBC	thermal barrier coating
YSZ	yttria-stabilized zirconia

1 (PDF)	DEFENSE TECHNICAL INFORMATION CTR DTIC OCA
1 (PDF)	CCDC ARL FCDD RLD DCI TECH LIB
7 (PDF)	CCDC ARL FCDD RLV P A GHOSHAL M WALOCK M MURUGAN L BRAVO R EMERSON C MOCK FCDD RLW MD M PEPI
2 (PDF)	CCDC AVMC R ARMSTRONG K KERNER
4 (PDF)	NAVAIR L SCHMIDT C ROWE C MYERS J SCITTORE
5 (PDF)	AFRL R SIKORSKI A KATZ D LEE R SONDERGAARD D BALLARD